ELECTRONIC SUPPLEMENTARY INFORMATION (ESI) for Mechanism for Formation of Atmospheric Cl Atom Precursors in the Reaction of Dinitrogen Oxides with HCl/Cl^- on Aqueous Films

Audrey Dell Hammerich,[*,†] *Barbara J. Finlayson-Pitts,*[‡] *R. Benny Gerber*[‡,§,||]

[†]Department of Chemistry, University of Illinois at Chicago, Chicago, Illinois 60607, United States

[‡]Department of Chemistry, University of California Irvine, Irvine, California 92697, United States

[§]Institute of Chemistry and the Fritz Haber Research Center, The Hebrew University, Jerusalem, 91904, Israel

[||]Laboratory of Physical Chemistry, P.O. Box 55, FIN-00014 University of Helsinki, Finland

This supplementary information gives results of electronic structure calculations and the BLYP-D3/TZV2P DFT study of this work on N_2O_5 systems and details the water slab model employed to simulate a thin film of water as well as the slab with N_2O_5 adsorbed. A comparison is made with geometrical properties determined via higher level DFT and non-DFT methods. Comparison is also made amongst different levels of theory in determining the effect of the size of the water cluster upon the geometry

of dinitrogen pentoxide. Finally properties of the model used for the film of water are characterized both with and without the oxide adsorbate.

Electronic Structure of N_2O_5. Table S1 lists equilibrium structural data for gaseous N_2O_5 in C_2 symmetry obtained from *ab initio* calculations employing density functional theory (mostly the B3LYP functional) and compares those results with the BLYP-D3/TZV2P data of this work (column 1) and the experimental gas phase electron diffraction values (column 2). Refer to Figure S1 for numbering of the atoms of dinitrogen pentoxide. The equilibrium structure given by the B3LYP functional reproduces the experimental values very well over a number of split-valence basis sets though B3LYP consistently overestimates the bridge N−O−N bond angle by 3° and underestimates the two torsions by a few degrees. The other BLYP study employed the TZ2P basis which is seen to be somewhat inferior to the current BLYP-D3/TZV2P study. However when TZ2P is combined with the B3PW91 functional, excellent agreement is obtained with the electron diffraction results. Table S2 gives the corresponding equilibrium structural data on N_2O_5 obtained via non-DFT methods, notably MP2, with one coupled cluster study and one quadratic configuration interaction study included. The MP2 results overestimate all bond lengths, underestimate the torsions, and generally underestimate bond angles. On average, B3LYP gives a better representation of the bond lengths and MP2 a better representation of the angles, including the torsions. Interestingly, the reported CCSD and QCISD calculations give bond lengths intermediate between the B3LYP and MP2 results, underestimate the bond angles more than MP2, and overestimate the main torsion.

For this current work, the BLYP-D3/TZV2P geometry yields bond lengths and bond angles which generally compare favorably with the experimental parameters

Table S1: Equilibrium Structure of Gas Phase N_2O_5 (C_2) Given by DFT Methods

parameter[a]	this work[b]	exp[c]	A[d]	B[e]	C[f]	D[g]	E[g]	F[h]	G[h]	H[i]
r(N1O1)	1.21	1.184	1.186	1.185	1.199	1.202	1.182	1.196	1.187	1.187
r(N1O2)	1.20	1.186	1.189	1.185	1.188	1.201	1.183	1.196	1.189	1.188
r(N1O5)	1.59	1.499	1.513	1.505	1.513	1.587	1.495	1.507	1.512	1.513
∠(O1N1O2)	134	134.2	133.5		133.8	134.1	133.4	133.2	133.4	133.5
∠(O1N1O5)	109			109.9				110.1	110.1	116.4
⟨∠(O1,2N1O5)⟩	113	112.8		113.3				113.4	113.3	113.3
∠(O2N1O5)	117			116.6				116.6	116.4	110.1
∠(N1O5N2)	116	112.3	115.2	115.4	115.3	117.4	115.1	114.7	115.0	115.1
d∠(O2N1O5N2)	23	33.7	∼ 30	29.0	29.7	21.1	31.6	28.6	28.5	28.7
d∠(O2O1N1O5)	3.6	5.0						3.4	3.4	4.3

[a] numbering of atoms given in Figure S1; bond lengths in angstroms, angles in degrees
[b] BLYP-D3/TZV2P gas phase geometry optimization
[c] gas phase electron diffraction values of Reference [1]
[d] B3LYP/6-311G(d,p) calculation of Reference [2]
[e] B3LYP/6-311++G(3df) calculation of Reference [3]
[f] B3LYP/6-311G(d) calculation of Reference [4]
[g] BLYP/TZ2P (D) and B3PW91/TZ2P (E) calculations of Reference [5]
[h] B3LYP/6-31+G(d) (F) and B3LYP/6-311++G(d,p) (G) calculations of Reference [6]
[i] B3LYP/6-311++G(d,p) calculation of Reference [7] (values for ∠(O1N1O5) and ∠(O2N1O5) may have been interchanged)

Table S2: Equilibrium Structure of Gas Phase N_2O_5 (C_2) Given by non-DFT Methods

parameter[a]	this work[b]	exp[c]	I[d]	J[e]	K[f]	L[g]	M[h]	N[i]	O[j]	P[k]
r(N1O1)	1.21	1.184	1.203	1.188	1.214	1.194	1.209	1.208	1.197	1.203
r(N1O2)	1.20	1.186	1.204	1.192	1.214	1.195	1.210	1.208	1.195	1.203
r(N1O5)	1.59	1.499	1.512	1.470	1.532	1.535	1.538	1.529	1.526	1.539
∠(O1N1O2)	134	134.2	133.3	132.9	133.6	134.0	134.0	133.8	133.9	134.0
∠(O1N1O5)	109		110.5	111.0	109.9		107.1	109.9	115.7	
⟨∠(O1,2N1O5)⟩	113	112.8	113.3		113.2		111.6	113.1	113.0	
∠(O2N1O5)	117		116.1		116.4		116.0	116.3	110.3	116.0
∠(N1O5N2)	116	112.3	110.8	111.6	112.7	112.5	111.4	111.8	111.8	111.5
d∠(O2N1O5N2)	23	33.7	35.6	36.8	31.3	32.0	29.7	32.0	31.7	
d∠(O2O1N1O5)	3.6	5.0	4.5	3.6			3.3	4.3	4.2	

[a] numbering of atoms given in Figure S1; bond lengths in angstroms, angles in degrees
[b] BLYP-D3/TZV2P gas phase geometry optimization
[c] gas phase electron diffraction values of Reference [1]
[d] CCSD(T)/aug-cc-pVDZ calculation of Reference [8]
[e] QCISD/6-311G(d) calculation of Reference [4]
[f] MP2/DZP calculation of Reference [9]
[g] MP2/TZ2P calculation of Reference [5]
[h] MP2/6-31+G(d) calculation of Reference [6]
[i] MP2/6-31G(d) calculation of Reference [10]
[j] MP2/6-311++G(d,p) calculation of Reference [7] (values for ∠(O1N1O5) and ∠(O2N1O5) may have been interchanged)
[k] MP2/aug-cc-pVDZ calculation of Reference [11]

(distances within 0.03 Å, angles within 4°) with one exception. The N−O bond of the N−O−N bridge is 6% too large. Both torsions are also underestimated though all reported calculations via B3LYP and MP2 similarly underestimate them. Overall the data in Tables S1 and S2 show that gas phase dinitrogen pentoxide can be considered to be two NO_2 groups joined by a common bridging O atom where the four atoms of each NO_3 grouping are nearly planar (5° torsion angle) with each NO_2 plane twisted with respect to the N−O−N plane in a contrarotary manner (34° torsion angle). Furthermore each N−O bond of the N−O−N bridge is rather long, ∼1.5 Å.

Electronic Structure of $N_2O_5(H_2O)_n$, n = 1 - 6. Due to the ability to perform higher level electronic structure calculations on them, water clusters are often employed as models for bulk water and for water surfaces. Table S3 gives data on N_2O_5 in clusters of 0, 1, 2, and 4 water molecules. Columns 1-5 are the BLYP-D3/TZV2P values of this work, column 6 the gas phase electron diffraction data, and columns 7-10 B3LYP/6-311++G(d,p) results. Row 7 gives an additional set of values for the N2−O5 bond length from an MP2/cc-pVDZ study on clusters of zero to two waters. The cluster results will be the initial focus and the water slab simulations addressed next. Taking the demonstrated superiority of B3LYP over second order Møller-Plesset perturbation theory in representing the bond lengths of dinitrogen pentoxide, one observes that MP2 also significantly overestimates the N2−O5 bonds in the clusters. For clusters of 0 – 2 waters the BLYP functional performs favorably with respect to B3LYP except it quite overestimates the bridging N2−O5 bond. For $N_2O_5(H_2O)_4$ the BLYP description is inferior and the N2−O5 bond poorly represented. Fortunately, as will be shown, this performance does not carry over to the water slab simulations. Nevertheless, the tabulated data definitely show that the size of the water cluster has a profound effect upon the equilibrium

Table S3: Effect of Water Cluster Size on the Equilibrium Structure of N_2O_5 (with Selected *asym*-N_2O_4 Data)

N_2O_5		number of waters					number of waters				*asym*-N_2O_4		
parameter[a]	slab[b]	4	2	1	0	exp[c]	0[d]	1	2	4	parameter[e]	slab	gas
r(N1O1)	1.21	1.26	1.23	1.22	1.21	1.184	1.187	1.19	1.20	1.21	r(N1O1)	1.26	1.23
r(N1O2)	1.21	1.26	1.24	1.23	1.20	1.186	1.188	1.19	1.21	1.22	r(N1O2)	1.26	1.22
r(N1O5)	1.62-1.63	1.31	1.40	1.45	1.59	1.499	1.513	1.47	1.40	1.35	r(N1O3)	1.33	1.47
r(N2O3)	1.21	1.19	1.19	1.19	1.21	1.184	1.187	1.18	1.17	1.16	r(N2O3)	2.16	1.74
r(N2O4)	1.21	1.18	1.18	1.19	1.20	1.186	1.188	1.18	1.17	1.16	r(N2O4)	1.12	1.14
r(N2O5)	1.62-1.63	2.16	1.84	1.77	1.59	1.499	1.513	1.56	1.67	1.78			
r(N2O5)[f]							1.54	1.73	1.77				
∠(O1N1O2)	134	123	128	130	134	134.2	133.5	132	129	127	∠(O1N1O2)	123	130
∠(O1N1O5)	110-113	117	113	111	109		116.4	110	112	114	∠(O1N1O3)	119	116
∠(O2N1O5)	113-116	119	119	119	117		110.1	119	119	119	∠(O2N1O3)	117	113
∠(O3N2O4)	134	142	140	138	134	134.2	133.5	135	138	142	∠(O3N2O4)	111	117
∠(O3N2O5)	110-113	98	104	106	109		116.4	108	105	103			
∠(O4N2O5)	113-116	109	116	116	117		110.1	117	116	115			
∠(N1O5N2)	116-117	119	118	118	116	112.3	115.1	118	120	118	∠(N1O3N2)	114	117

[a] numbering of atoms given in Figure S1; bond lengths in angstroms, angles in degrees

[b] BLYP-D3/TZV2P calculation of this work: column 1 – range for 42 ps 278 K, 45 ps 292 K and 43 ps 322 K N_2O_5/water slab trajectories, each averaged over and equivalent bonds/angles averaged over; columns 2-5 – gas phase geometry optimization of N_2O_5 with 4, 2, 1, and 0 waters

[c] column 6 – gas phase electron diffraction values of Reference [1]

[d] B3LYP/6-311++G(d,p) calculation of Reference [7] (except row 7 as noted below): columns 7-10 – clusters of N_2O_5 with 0, 1, 2, and 4 waters; angles given for clusters containing water calculated from coordinates reported by the authors (values for ∠(O1N1O5) and ∠(O2N1O5) may have been interchanged in column 7)

[e] BLYP-D3/TZV2P calculation of this work on N_2O_4, selected data: columns 1 and 2 – final 30 ps of a 60 ps 307 K N_2O_4/water slab trajectory and gas phase geometry optimization, respectively

[f] MP2/cc-pVDZ calculation of Reference [12]: columns 7-9 – clusters of N_2O_5 with 0 – 2 waters

geometry of N_2O_5. As more waters are added the N−O bonds of one of the terminalNO_2 groups shortens, its O−N−O angle increases, its two O−N−O angles involving the bridging oxygen decrease, and its N−O bond with the bridging oxygen significantly lengthens. Exactly the opposite behavior is found for the bonds and angles involving the NO_2 group on the other side of the molecule. Clearly, in clusters, the waters are inducing a pronounced asymmetry to these two parts of the molecule. Examining the cluster structures given in Figure S1, one finds that the behavior for the NO_2 group whose bridge N−O bond lengthens has its N atom involved in an intermolecular interaction with a water oxygen. On the other hand the NO_2 group with a shortening bridge N−O is associated with water which is hydrogen bonding to one (or more) of the NO_2 oxygen atoms. These interactions should lead to a significant polarization of the molecule.

Water Induced Charge Separation of N_2O_5 in Water Clusters. As the electronic structure calculations show, the two NO_2 groups of dinitrogen pentoxide are equivalent; the respective bond lengths and bond angles are identical. However, the equivalence can be broken in an asymmetric environment such as that provided by water, as Table S3 indicates. Table S4 gives data illustrating the effect of the size of the water cluster on fostering this asymmetry in terms of the two bridge N−O bonds lengths and Mulliken charges on the now nonequivalent nitryl groups which will be shown to parcel into $NO_2^{\delta+}$ and $NO_3^{\delta-}$ fragments. Though the two nitryl groups in gaseous N_2O_5 are equivalent, one can still formally add all the Mulliken partial atomic charges on one of the NO_2's atoms and do the same for the remaining NO_3 atoms. These charges represent the fragment charges for N_2O_5 with no waters and are given in the first four rows of N_2O_5 data in the table. The data in the table derive from five distinct calculations done at various levels of theory employing different basis sets so

Table S4: Effect of Water Cluster Size on Geometry and Charge Polarization in N_2O_5[a,b]

	NO_3 fragment			NO_2 fragment		
cluster	N1−O5	$O_2NO\cdots HOH$[c]	charge[d]	N2−O5	$O_2N\cdots OH_2$[e]	charge[d]
N_2O_5[f,g]	1.59		−0.10	1.59		0.10
	1.51		0.08	1.51		−0.08
	1.54		−0.13	1.54		0.13
	1.51		−0.19	1.51		0.19
$N_2O_5(H_2O)$[f]	1.45	2.22	−0.25	1.77	2.86	0.25
	1.47		0	1.56	2.79	0.06
			−0.28	1.73	2.66	0.27
$N_2O_5(H_2O)_2$[f]	1.40	2.02	−0.32	1.84	2.71	0.32
	1.40	2.12	−0.12	1.67	2.71	0.18
		2.02	−0.32	1.77	2.59	0.33
$N_2O_5(H_2O)_4$[h]	1.31	1.89, 1.91	−0.53	2.16	2.12	0.32
	1.22	2.01, 2.15	−0.25	1.78	2.56	0.29
	1.45	2.01	< 0.07[i]	1.52	2.48	0.18

[a] refer to Figure S1 for designation of numbering for atoms in bonds and identification of atom involved in H bond or intermolecular interaction with water

[b] first row of data for each cluster – BLYP-D3/TZV2P values of this work; second row – B3LYP/6-311++G(d,p) calculation of Reference [7]

[c] hydrogen bond length between water and an O atom of NO_3 fragment; two O atoms of NO_3 fragment each have a water H bonded in the first two four-water cluster data sets

[d] sum of Mulliken partial atomic charges in fragment in au

[e] intermolecular interaction distance between water O and N atom of NO_2 fragment

[f] third row – MP2/cc-pVDZ calculation of Reference [12]

[g] fourth row – B3LYP/6-311++G(3df) calculation of Reference [3]

[h] third row – HF/3-21G calculation of Reference [13]

[i] omits partial atomic charge of negative bridge oxygen

that the magnitudes of the Mulliken charges can be expected to be different in each calculation. Nevertheless the more complete sets of data given by this work and the B3LYP and MP2 studies show that each additional water added to the cluster: 1)

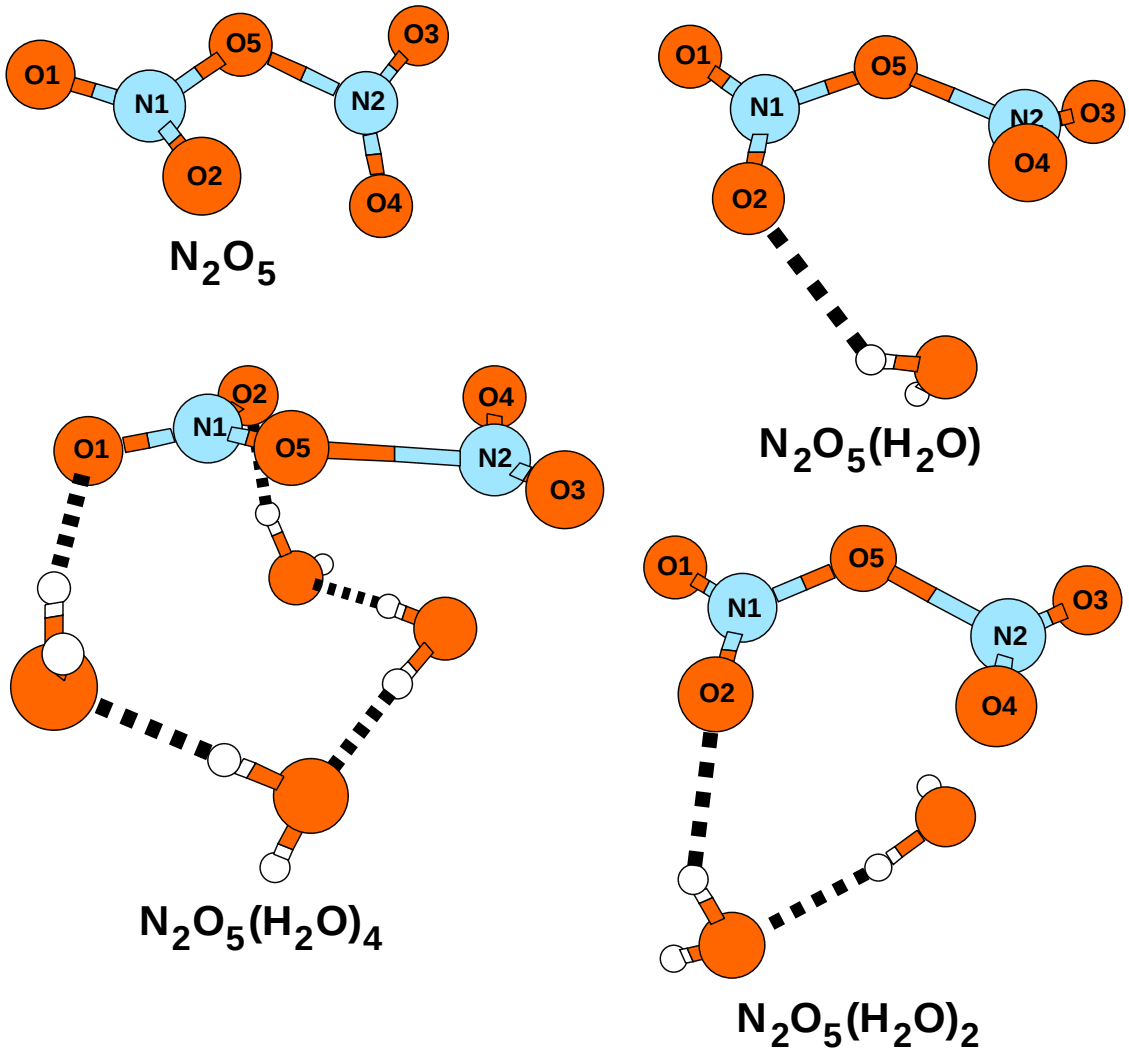

Figure S1: N_2O_5 and model water clusters examined to compare results with higher level *ab initio* calculations. Numbering provides the key for Tables S1-S4. Note that $N_2O_5(H_2O)_4$ has a different orientation from N_2O_5 and N_2O_5 in the other two clusters.

increases the charge on the NO_2 fragment, 2) has an oxygen which participates in an intermolecular interaction with NO_2's N atom of increasingly shorter range, and 3) dramatically increases the fragment's bridge N−O bond length. On the other hand, for the NO_3 fragment, as the number of waters increases 1) the NO_3 charge decreases, 2) a hydrogen bond with the fragment forms of increasingly shorter H-

bond length, and 3) the fragment's bridge N−O bond length decreases. Data from the other two calculations fill in this trend. Clearly water is inducing an ionization or partial ionization into two fragments, $NO_2^{\delta+}$ and $NO_3^{\delta-}$. This fragment partitioning explains the water-induced geometry changes noted for the two NO_2 groups in the previous section. Whether this is indicative of the ionization of eqn (1) in the main text (actually disproportionation), the ion pairing of eqns (2)-(4), or something in between will be examined further.

Water Slab as a Model for a Thin Film of Water. It is possible that the aqueous "surface" upon which the dinitrogen oxides of this study react with HCl/Cl^- are thinner than the slabs used in these simulations [14]. Consequently, in modeling the film, a thick slab where perfectly converged properties could be obtained was not an objective. Nevertheless, DFT via BLYP-D3/TZV2P, including dispersion, has been shown to give a good description of water and the liquid/vapor interface [15–17]; the quality of this description was sought for the thin slabs employed here. Of particular concern was generation of a slab whose water was not overstructured and was sufficiently mobile.

Figure S2 exhibits the density profile and diffusive behavior of the bare water slab and the slab with a molecule of dinitrogen pentoxide adsorbed. From a fit of the profile to a hyperbolic tangent function, the density and Gibbs dividing surface z_{GDS} (height above slab in the interfacial region where the density of molecules in the vapor and liquid are equal) are given. The upper and lower dividing surfaces define the slabs to be 10 Å thick with a density a little in excess of 1 g cm^{-3}. While the simulations are done with deuterium rather than protium, the density is calculated for protiated water to facilitate comparison. The corrugation observed in the profiles is normal for finite

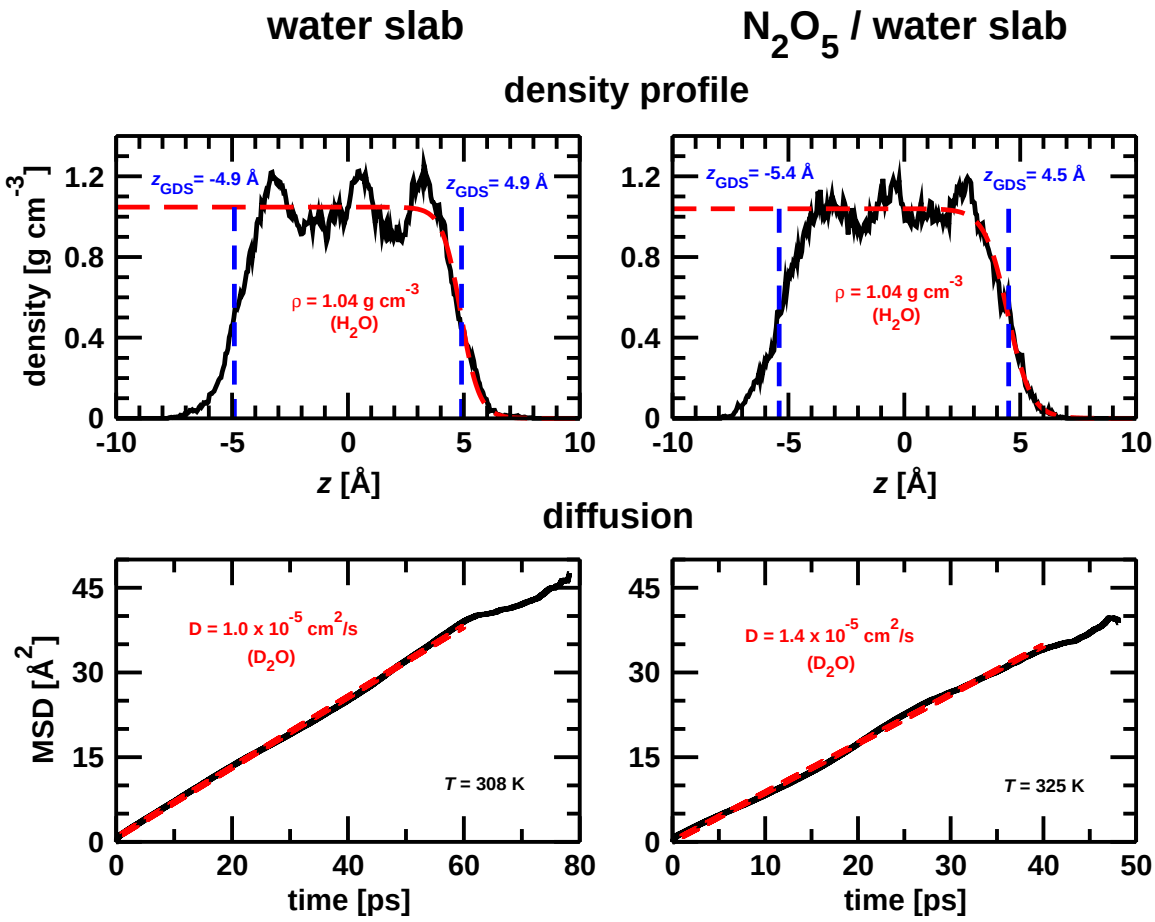

Figure S2: Comparison of density profile and diffusive behavior of bare water slab and the slab with a molecule of N_2O_5 adsorbed. Dashed red line in profile denotes fit of density to a hyperbolic tangent and dashed blue line Gibbs dividing surface for the upper and lower side of each slab given by the fit. Diffusion constants for water in lower panels determined from a linear fit (dashed red line) to the slope of the mean square displacement as a function of time using the Einstein relation, ignoring later times when statistics are poorer.

sized systems and more modest than most reported. The N_2O_5 adsorbate exhibits little perturbation of the profile. The lack of symmetry in placement of the upper and lower z_{GDS} is attributable to mass weighting of the z coordinate, height above or below the center of mass for the slab. As deuterium is employed in the simulations, the water self-diffusion constants D reported are calculated from the slope of the

mean square displacement of all oxygen atoms of D_2O over the entire slab, suitably averaged over initial times and time intervals. The factor of 1.4 upon increasing the temperature from 308 to 325 K is exactly what is experimentally observed. However, the constants for the bare slab and slab with N_2O_5 are a factor of 2.4 times smaller than experimentally reported values for bulk liquid D_2O, (2.38 and 3.43) $\times$ 10^{-5} cm^2 s^{-1} at 308 and 325 K, respectively [18]. Though the true D for a thin film is neither known nor experimentally available, frequently AIMD simulations yield reduced diffusion coefficients for bulk systems attributable to the necessity of very long trajectories ($\sim$ 170 ps!) to overcome the nonergodic behavior of NVE simulations [19, 20]. The water slab was equilibrated in the NVT ensemble for 50 ps and data collected for 78 ps from an NVE trajectory. 20 ps of canonical equilibration was performed for the slab with N_2O_5 adsorbed. Though the magnitude of the diffusion constant may be lower than the true value, D responds to temperature increments in the appropriate manner and shows that the water molecules possess decent mobility. Furthermore, the water does not exhibit any significant overstructuring.

N_2O_5 Adsorbed onto a Thin Film of Water. Table S3 gives structural parameters for gaseous N_2O_5, clusters of gaseous N_2O_5 with 1, 2, and 4 water molecules, and N_2O_5 adsorbed onto a water slab. Selected data for gas phase N_2O_4 and N_2O_4 adsorbed onto a slab are included for comparison of the effects of water, especially on the slab, on both of these dinitrogen oxides. As with all of the electronic structure calculations, this study shows increasing lengthening of the bridging N1$-$O5 or N2$-$O5 bond with number of waters incorporated into the cluster. It was noted previously that the BLYP-D3/TZV2P data for a cluster with 4 waters has an exceedingly long bridge N2$-$O5 bond length (2.16 Å) as Table S4 also indicates. This could pose a problem with the DFT description. Fortunately, a comparison of slab simulation

data of column 1 in Table S3 with gas phase data of column 5 shows only a modest relaxation in N_2O_5's structure upon adsorption onto an aqueous film with a bridging bond extension of 0.03 – 0.04 Å. The data in column 1 give ranges for averaging the coordinate parameter over the trajectory and over the two equivalent NO_2 groups in each of three trajectories spanning a 45 K temperature variation. Though the average value of a bond length or angle is not sensitive to temperature, the value itself exhibits oscillatory behavior as a function of time whose period is temperature dependent. These oscillations are displayed in the O_2NO-NO_2 bond in Figure 1 of the main article and lead to an identical periodicity (or mirror image periodicity) in Mulliken charges of the NO_2 and NO_3 fragments of N_2O_5. Such periodic motion is absent for *asym*-N_2O_4 adsorbed onto a slab surface.

Red and black curves in the left panels of Figure S3 explore the temperature dependent oscillatory nature of Mulliken charges for N_2O_5. Green curves give the sum of all partial atomic charges in dinitrogen pentoxide; the value of -0.02 au indicates a consistent small amount of charge transfer from surrounding water molecules at all three temperatures. For all three traces maxima in black correspond to times when N1 bears the largest $NO_2^{\delta+}$ charge and N2 the smallest $NO_3^{\delta-}$ charge (most negative); maxima in red indicate when N2 bears the largest $NO_2^{\delta+}$ and N1 the smallest $NO_3^{\delta-}$ charges. Values reported for the fragments are averaged by assigning the NO_2 and NO_3 fragments to each N. As stated in the previous paragraph, various structural parameters also display a periodic nature correlated with charge separated fragments. When a fragment achieves its maximum $NO_2^{\delta+}$ character the bridge N−O bond lengthens to 1.79 Å, the O−N−O angle to 139° while the N−O bond length shortens to 1.19 Å and the torsion angle is 25° (angle between the NO_2 planes is 50°). On the other hand, maximum $NO_3^{\delta-}$ character exhibits a bridge N−O bond reduction to 1.47

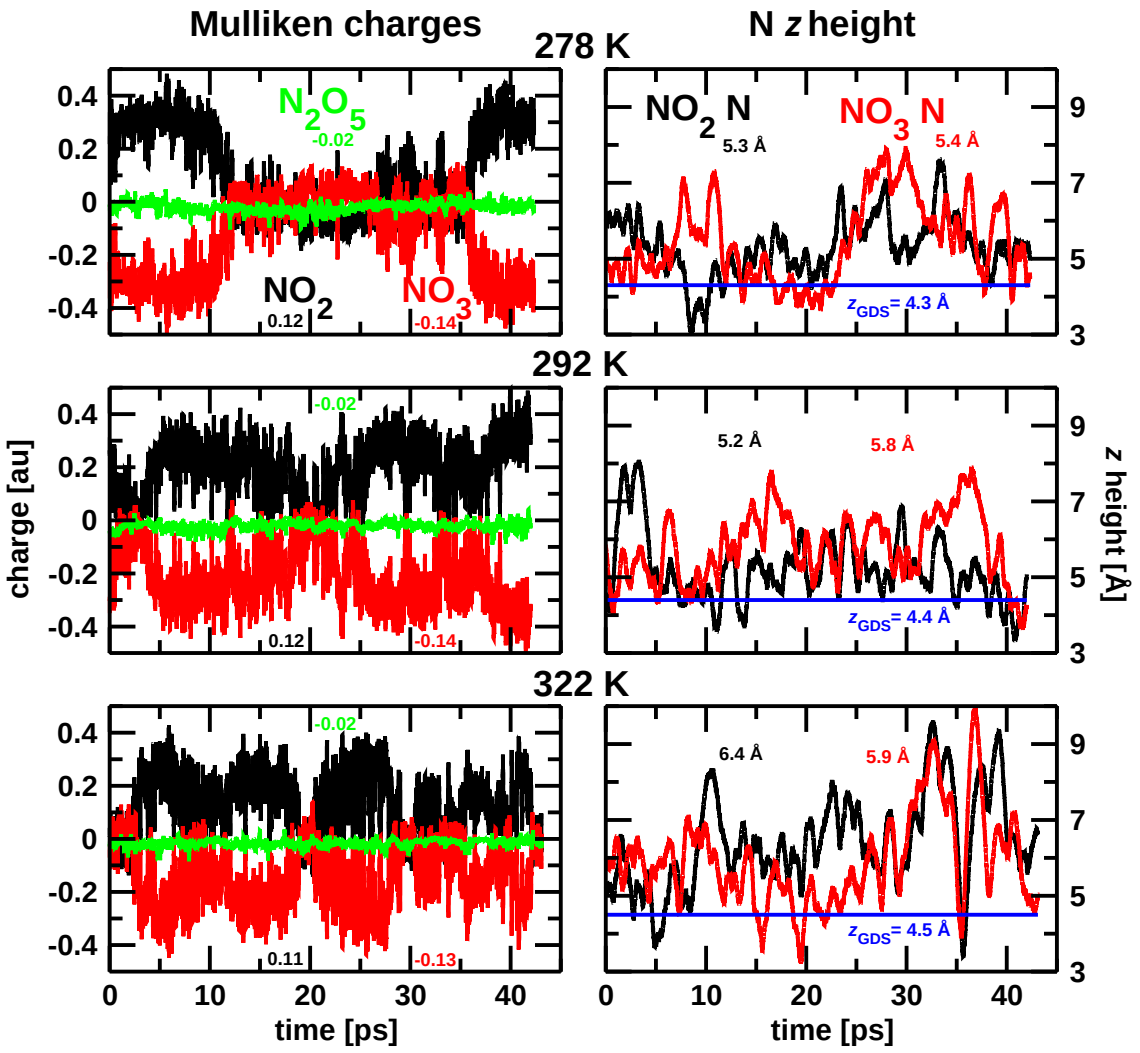

Figure S3: Time evolution of Mulliken partial atomic charges in au of the NO_2 (in black) and NO_3 (in red) fragments and height of N atom in each fragment above slab surface. For each simulation the Gibbs dividing surface is denoted by the blue horizontal line. Data reported for a 42 or 43 ps time interval in each trajectory with red and black values averages for the respective quantity over the interval.

Å, an O−N−O angle to 130° with an N−O bond length increase to 1.23 Å and the torsion increases to 65° (130° between planes). In this study the solvated nitrate ion product has a bond length of 1.28 Å, angle of 120°, and Mulliken charge of −0.8 au. Examination of the slab column data for *asym*-N_2O_4 in Table S3 suggests that, with

a 1.26 Å N−O bond length, 123° bond angle, and charge of −0.54 au (from Table 1 of main text) on a thin film of water $ONONO_2$ exhibits more ion pair character than N_2O_5 at the temperatures simulated. However, the frequency of N_2O_5's periodic motion is seen to decrease with temperature in Figure S3 with periods of about 10, 16, and 45 ps approximated by fitting to a sine function. It must be remembered that the limiting behavior with decreasing temperature is a lack of oscillatory structure and two permanently charged separated fragments, consistent with the known existence of N_2O_5 as an ionic crystal consisting of NO_2^+ and NO_3^- ions at low temperatures.

The height of each N atom above the surface upon which N_2O_5 is absorbed is also given as a function of temperature in Figure S3. Values of the height are from the center of mass and can be compared to the position of the Gibbs dividing surface shown in blue. These lead to average values above z_{GDS} of 1.1, 1.1, and 1.7 Å with increasing temperature. As is to be expected, as temperature increases the slab expands resulting in the increase in z_{GDS}. (For the lower surface z_{GDS} = 5.2, 5.2, and 5.4 Å and the respective slabs are 9.5, 9.5, and 9.9 Å thick). Large amplitude motions of the NO_2 and NO_3 fragments are seen to increase somewhat with temperature. However no discernible difference in position of either of the N atoms above the surface is observed, another indication of the long-time equivalence of the nitrogens.

REFERENCES FOR SUPPORTING INFORMATION

[1] McClelland, B. M.; Richardson, A. D.; Hedberg, K. A. *Helv. Chim. Acta* **2001**, *84*, 1612.

[2] Jaroszyńska-Wolińska, J. *J. Mol. Struct.* **2010**, *952*, 74.

[3] Zakharov, I. I.; Kolbasin, A. I.; Zakharova, O. I.; Kravchenko, I. V.; Dyshlovoi, V. I. *Theo. Exp. Chem.* **2007**, *43*, 66.

[4] Grabow, J.-U.; Andrews, A. M.; Fraser, G. T.; Irikura, K. K.; Suenram, R. D.; Lovas, F. J.; Lafferty, W. J. *J. Chem. Phys.* **1996**, *105*, 7249.

[5] Munakata, H.; Kakumoto, T.; Baker, J. *J. Mol. Struct.* **1997**, *391*, 231.

[6] Hanway, D.; Tao, F.-M. *Chem. Phys. Lett.* **1998**, *285*, 459.

[7] McNamara, J. P.; Hillier, I. H. *J. Phys. Chem. A* **2000**, *104*, 5307.

[8] Glendening, E. D.; Halpern, A. M. *J. Chem. Phys.* **2007**, *127*, 164307.

[9] Bencivenni, L.; Sanna, N.; SchriverMazzuoli, L.; Schriver, A. *J. Chem. Phys.* **1996**, *104*, 7836.

[10] Parthiban, S.; Raghunandan, B. N.; Sumathi, R. *J. Mol. Struct.* **1996**, *367*, 111.

[11] Voegele, A. F.; Tautermann, C. S.; Loertingy, T.; Liedl, K. R. *Phys. Chem. Chem. Phys.* **2003**, *5*, 487.

[12] Raff, J. D.; Njegic, B.; Chang, W. L.; Gordon, M. S.; Dabdub, D.; Gerber, R. B.; Finlayson-Pitts, B. J. *Proc. Natl. Acad. Sci. U.S.A.* **2009**, *106*, 13647.

[13] Bianco, R.; Hynes, J. T. *Int. J. Quant. Chem.* **1999**, *75*, 683.

[14] Finlayson-Pitts, B. J. *Phys. Chem. Chem. Phys.* **2009**, *11*, 7760.

[15] Kühne, T. D.; Pascal, T. A.; Kaxiras, E.; Jung, Y. *J. Phys. Chem. Lett.* **2011**, *2*, 105.

[16] Baer, M. D.; Mundy, C. J.; McGrath, M. J.; Kuo, I.-F. W.; Siepmann, J. I.; Tobias, D. J. *J. Chem. Phys.* **2011**, *135*, 124712.

[17] Jonchiere, R.; Seitsonen, A. P.; Ferlat, G.; Saittal, M.; Vuilleumier, R. *J. Chem. Phys.* **2011**, *135*, 154503.

[18] Hardy, E. H.; Zygar, A.; Zeidler, M. D.; Holz, M.; Sacher, F. D. *J. Chem. Phys.* **2001**, *114*, 3174.

[19] Lee, H.-S.; Tuckerman, M. E. *J. Chem. Phys.* **2007**, *126*, 164501.

[20] Ding, Y.; Hassanali, A. A.; Parrinello, M. *Proc. Natl. Acad. Sci. U.S.A.* **2014**, *111*, 3310.